Atomistic Simulation of a Glassy Polymer/Graphite Interface

Kevin F. Mansfield and Doros N. Theodorou*

Department of Chemical Engineering, University of California, Berkeley, and Center for Advanced Materials, Lawrence Berkeley Laboratory, Berkeley, California 94720

Received January 4, 1991

ABSTRACT: A computer simulation technique has been developed that is capable of probing the interface between an amorphous glassy polymer and a crystalline solid substrate in atomistic detail. The interface between bulk glassy atactic polypropylene and a graphite basal plane is used as a test case. The method requires the generation of a set of static model microstates that are in detailed mechanical equilibrium, each characterized by two-dimensional periodic boundary conditions and consisting of multiple chains of polymer sandwiched between two semiinfinite solid phases. To obtain a static model microstate, an initial guess microstate is first generated by a Monte Carlo procedure based on the rotational isomeric state model with corrections for long-range interactions. Subsequently, the total potential energy is minimized with respect to all microscopic degrees of freedom. From such a set of static model microstates, we have predicted the internal energy contribution to interfacial thermodynamic properties, as well as the local structural features. A quantitative estimate for the work of adhesion between atactic polypropylene and graphite has been obtained, which agrees well with experiment. The distribution of local internal stresses confirms that microstates are mechanically isotropic in their middle region (far from the solid surfaces), which is indistinguishable from unperturbed bulk polymer. The local structure of the polymer lying within 10 Å of a graphite surface is found to be different in many ways from that of the corresponding bulk. Near the solid, the local polymer density profile displays a maximum, the backbone bonds of chains develop considerable orientation parallel to the solid surface, and the usually preferred trans rotational state is suppressed. Adsorbed pendant hydrogens of the polymer concentrate preferentially on top of the centers of the hexagons in the graphite honeycomb. The polymer structure has been explored at the level of entire chains as well. The chain center of mass distribution diplays a maximum approximately 1 unperturbed root-mean-squared radius of gyration away from each solid surface. Chains orient with their longest dimension parallel to the graphite phases. The intrinsic shape of the chain segment clouds, as characterized by spans and principal moments of inertia, is found not to be a strong function of position relative to the interface. All polymer/solid results presented have been screened for possible system size effects and compared to the corresponding results from a recent computer simulation of the free surface of glassy atactic polypropylene.

1. Introduction

Polymer/solid interfaces are very important in a wide variety of technologies. They are encountered in adhesives and protective coatings, as well as lubricants and suspension stabilizers.[1] The structure, thermodynamic, and mechanical properties of the polymer/solid combination play a significant role in dictating the overall performance of the multiphase material system. An example involving glassy polymers is provided by state-of-the-art polymeric composites. The stiffness, toughness, and strength of the individual phases (polymeric matrix and solid filler) are extremely important in shaping the overall mechanical behavior of the composite. However, failure is often observed to start in the interfacial region. It may be either interfacial or cohesive and still be affected by the interface. Breakdown of the interphase can occur for many reasons such as the existence of differences in thermal expansion coefficients, the migration of water to the interface, or the poor physical and/or chemical attachment of polymer to the solid phases. The work of adhesion,[2] W_a, provides a quantitative thermodynamic measure of the strength of attachment at the interface. Experimental studies of adhesive failure have shown that the strain energy release rate[1] associated with the propagation of a crack between polymer and solid phases, although strongly rate dependent because of contributions of plastic and viscoelastic deformation of the polymer, is always proportional to the work of adhesion.

To judiciously select and efficiently design materials for use in the above areas of technology, we need to understand polymer interfacial behavior *at the molecular level*. Interfaces are intrinsically inhomgeneous and anisotropic. There is an asymmetry between cohesive interactions within the polymer and adhesive interactions between the polymer and the adjacent phase. In addition, chain conformations experience strong entropic constraints at a phase boundary, against which they cannot propagate. These factors cause the organization and shape of macromolecules at the interface to be quite different from those in the bulk. Perturbations in structure relative to the bulk polymer, in turn, govern all the macroscopic interfacial properties that one would wish to control and manipulate.

Computer simulation has been used extensively to study the energetics and molecular structure of fluid phases near flat solid surfaces. Early work in the field developed potentials for the description of the physical interaction between a single adsorbing atom (adatom) and a structureless wall.[3,4] In this work, solids are viewed as semiinfinite assemblages of ordered molecules that interact with the single adatom through pairwise additive potentials, such as the Lennard-Jones potential. These pairwise interactions, which are infinite in number, are frequently summed through integration by smearing the solid atoms either in layers (10–4 potential) or in all three dimensions (9–3 potential). More elaborate potential summation methods were developed for atomistically explicit ("corrugated") model surfaces of known geometry, such as graphite basal planes and the (100) and (111) faces of an fcc lattice. Significant progress toward developing interatomic interaction potentials for rare gas atoms next to these solid phases,[5-7] including three-body contributions in the adatom/graphite potential,[8] has been accomplished.

* To whom correspondence should be addressed at the University of California, Berkeley.

0024-9297/91/2224-4295$02.50/0 © 1991 American Chemical Society

These potentials have been used extensively in computer simulations to study single-atom adsorption as well as monolayer and multilayer formation by physisorption from the gas phase on simple solid surfaces. Some systems studied include argon,[9] krypton,[10,11] methane,[12,13] ethane,[14] ethylene,[15] butane and decane,[16] nitrogen,[17-19] chlorine,[20] ammonia,[21] several aromatics,[22,23] and single epitaxially deposited polyethylene chains.[24] Computer simulations of simple liquids in the presence of structureless walls have been performed by molecular dynamics[25] and Monte Carlo techniques.[26] In addition, liquids such as argon[27,28] and *n*-hexane[29] have also been explored near corrugated surfaces. Recently, there has been significant interest in simulating macromolecular liquids near solid surfaces. The model system is typically a low molecular weight analogue of polyethylene, represented as a string of beads between featureless solid walls, which may be energetically neutral or attractive toward the beads. Various structural and dynamic aspects have been probed by using lattice Monte Carlo,[30-33] off-lattice Monte Carlo,[34-36] and molecular dynamics techniques.[37] Other types of polymer/solid interfaces have also been studied computationally. Lattice and off-lattice simulations of layers of chains terminally attached to structureless walls in a solvent,[38-40] as well as lattice simulations of polymer/polymer interfaces, are important examples.[41] Off-lattice Monte Carlo has been used to examine a spherical micelle of amphiphilic molecules and a droplet of tridecane molecules,[42] and lattice-based dynamic calculations have been employed to probe the adsorption and aggregation of dissolved copolymer molecules near smooth or rough surfaces.[43] All computer simulations for polymer chains reported so far treat the chains as assemblages of simple spheres (united atom representation) connected by springs or stiff bonds and use highly idealized smooth solid models. These simplifications render the simulations capable of providing coarse-grained information on the local chain structure and organization at an interface but do not allow the quantitative prediction of interfacial thermodynamic properties such as the work of adhesion. In addition, no simulation work has yet been reported on glassy polymers at solid surfaces.

Computer simulations of bulk glasses have been reported. Andersen has used molecular dynamics to study the glass transition of atomic argon and the structure of resulting glasses.[44] Recently, Rigby and Roe have extended this approach to macromolecular glasses of short polyethylene-like chains.[45] Several molecular mechanics-based atomistically detailed computer simulations of bulk phases of glassy polymers have appeared. Polymers studied include atactic polypropylene (PP),[46] atactic poly(vinyl chloride) (PVC)[47], and Bisphenol A polycarbonate.[48] PP has also been subjected to molecular dynamics simulations.[49] Previous bulk work[46] has recently been extended to explore interfacial systems involving glassy polymers in the same atomistic detail. The free surface of glassy atactic polypropylene, i.e., a polymer/vacuum interface, was used as an example to demonstrate our new approach.[50] The results from this work included a prediction for the internal energy contribution to surface tension that is within 7% of the experimental value. In addition, a wealth of molecular-level structural information was obtained. The local density profile at the surface was found to be sigmoidal. Perturbations from isotropy in the local density, bond orientation, and bond torsion angle distribution were seen over an interfacial region of thickness approximately equal to 10 Å. Structural features at the level of entire macromolecules were also explored. Chains whose center of mass is located near the surface were found to orient flat, with their longest dimension parallel to the film plane. The overall shape of chain segment clouds, as characterized by the spans and principal moments of inertia, was not found to deviate significantly from chain shape in the bulk polymer glass.

The objective of the work reported here is to apply computer simulation to a well-defined glassy polymer/solid interface, in order to understand and predict (I) microscopic structural features in the interfacial region, such as density distribution, bond orientation, chain shape, rotation angle distribution, and organization of adsorbed groups on top of the solid surface and (II) macroscopic thermodynamic properties such as adhesion tension and work of adhesion. Our approach is distinguished from other polymer/solid simulation work in that we use a detailed atomistic representation of the polymer and solid phases, which corresponds as closely as possible to the real system under examination. This level of representation allows the quantitative prediction of actual values for interfacial thermodynamic properties that can be tested against experiment. Our work focuses on polymers in the glassy state, as opposed to polymer melts. Furthermore, we have designed our approach for maximal computation efficiency by taking advantage of the computer hardware available to us and carefully choosing the approximations underlying our theoretical formulation. We have extended our earlier glassy polymer/vacuum methodology[50] to glassy atactic polypropylene adhering to basal planes of graphite.[51] Graphite was chosen as the solid substrate because of its relevance in composite applications.[2] Its surface properties have been extensively studied experimentally; also, its interactions with polypropylene are largely of a London dispersion type and can be described satisfactorily in terms of existing potential expressions.[5] This polymer/solid combination constitutes one of the simplest real systems one could examine where uncertainties in the interaction potentials are minimal, thus allowing for a stringent test of the methodology. The simulation method we describe in the following sections is perfectly general and applicable, in principle, to the interface between any glassy polymer and any solid phase, provided the molecular structures of all components are known and appropriate interatomic interaction potentials are available. The underlying physical picture is that of a polymer glass created by slow vitrification of the melt, while in contact with the solid phases. The microscopic model we have developed is described in section 2 of this paper. Our simulation methodology is discussed in section 3. The results are presented in section 4 and include the prediction of two thermodynamic properties (the internal energy contributions to the work of adhesion and to the adhesion tension), as well as microscopic structural features. Finally, our findings are summarized in section 5. Mathematical details of the formulation are elaborated in the Appendix sections.

2. Model

Our molecular model rests on the following assumptions.[46,50] Local regions of a polymeric glass are viewed as fluctuating around configurations satisfying the conditions of detailed mechanical equilibrium, i.e., constituting *local* minima of the total potential energy in configuration space. We will call such minimum energy configurations "static model microstates". Transitions from the vicinity of one local minimum to the vicinity of another are extremely unlikely over ordinary time scales, due to the high potential energy barriers between minima. The thermodynamics

of a region of the glass fluctuating in the vicinity of a static model microstate is developed in a harmonic approximation. Estimates of the macroscopic properties of the entire glass are then obtained by arithmetically averaging the corresponding properties of local regions locked in the vicinity of different microstates. In this analysis, the minimum energy microstates become the focus of attention, and generating them becomes a central objective of the simulation. We have developed a computational procedure for the creation of static model microstates, to be described in detail in the following section. As a result of this procedure the microstates have an average bulk density (i.e., density in the middle region, which lies sufficiently far from interfaces) that is consistent with the experimental density of a well-relaxed polymer glass at the temperature and pressure of interest. In reality, the distribution of minimum energy microstates representative of local regions in a glassy polymer would depend on the history of vitrification. We assume that our computational process of generating static model microstates yields a sufficiently accurate representation of the actual distribution of local environments within a polymer glass formed by slowly cooling a melt. It is noteworthy that the distribution of potential energy over the static model microstates is quite narrow, its standard deviation not exceeding 0.04 kT/atom. The reader should also note that our static model microstates are not 0 K states. Since they are created under specific temperature and pressure conditions, they are inherently different from the 0 K minima probed by Stillinger and Weber in their studies of small molecular weight amorphous materials.[52] In our solid/polymer simulations, the polymer is assumed to be glassy throughout the model system, up to the solid surfaces. This is reasonable, since attractive interactions with the solid will give rise to regions of enhanced density, hence of even lower molecular mobility than the polymer bulk (see section 4).

Our statistical mechanical analysis of a local region fluctuating in the vicinity of a local potential energy minimimum, in a harmonic approximation with respect to all microscopic degrees of freedom, leads to the following useful result.[46,50] The derivative of the internal energy $\underline{U}$ with respect to any space-related thermodynamic quantity ξ, such as volume, strain, or surface area, can be well estimated by the corresponding derivative of potential energy $\mathcal{V}^0$ at the local minimum:

$$\left.\frac{\partial^m \underline{U}}{\partial \xi^m}\right|_{T,\xi'} = \left.\frac{\partial^m \mathcal{V}^0}{\partial \xi^m}\right|_{\xi'} \tag{1}$$

The thermodynamic properties of the considered region can now be expressed in terms of the dependence of the potential energy on the spatial extent of the system. Equation 1 allows one to calculate the internal energy contribution to thermodynamic quantities, such as adhesion tension and work of adhesion, from configurational characteristics of our static model microstates.

Our molecular model employs a realistic representation of molecular geometry and energetics. Bond lengths and bond angles of the polymer are treated as classical springs of infinite stiffness, following the "classical flexible" model of Gō and Scheraga.[53] Thus, molecular rearrangement can occur through overall chain translation and rotation and through torsion around skeletal bonds. Skeletal carbons, pendant hydrogens, and methyl groups are treated explicitly. They interact with one another through Lennard-Jones potentials, whose parameters are taken from the recommendations of Bondi, Suter, and Flory.[54,55] In addition there is an intrinsic torsional potential associated with skeletal bonds.[55,56] Our potential representation and our method for calculating the polymer/polymer contribution to the potential energy are identical with those used in our previous work on bulk phases[46] and free surfaces[50] of glassy atactic polypropylene. In the present simulation, the polymer is exposed to semiinfinite graphite phases terminating in basal planes perpendicular to the z coordinate axis. The graphite phases are represented as sets of Lennard-Jones carbon centers at their crystallographically correct positions. The solid structure is assumed to remain unperturbed by the adsorption of polymer. For each atom in the polymer, an interaction potential due to all atoms in each semiinfinite solid phase is included in the total potential energy function.

To calculate the potential energy of interaction, $\mathcal{V}^W$, between a polymer atom at position r and a semiinfinite graphite phase, we implement an efficient and accurate Fourier summation method designed by Steele,[5] which takes advantage of the symmetry in the crystalline substrate:

$$\mathcal{V}^W(r) = \mathcal{V}_0(z) + \sum_{n>0} \mathcal{V}_n(z) f_n(s1,s2) \tag{2a}$$

and $\mathcal{V}_0$ and $\mathcal{V}_n$ are defined as

$$\mathcal{V}_0(z) = \frac{4\pi\sigma_{ps}^2\epsilon_{ps}}{a_s}\sum_{\alpha=0}^{\infty}\left[\frac{2}{5}\left(\frac{\sigma_{ps}}{z+\alpha d}\right)^{10} - \left(\frac{\sigma_{ps}}{z+\alpha d}\right)^4\right] \tag{2b}$$

$$\mathcal{V}_n(z) = \frac{2\pi\sigma_{ps}^6\epsilon_{ps}}{a_s}\left[\frac{\sigma_{ps}^6}{30}\left(\frac{g_n}{2z}\right)^5 K_5(g_n z) - 2\left(\frac{g_n}{2z}\right)^2 K_2(g_n z)\right] \tag{2c}$$

σ_{ps} and ϵ_{ps} are the collision diameter and well depth, respectively, of the Lennard-Jones potential describing the pair interaction between the polymer atom and a graphite carbon. s1 and s2 define the x and y coordinates of the projection of the polymer atom upon the first layer of graphite atoms relative to the surface unit cell of graphite and range from 0 to 1. The area of the surface unit cell is a_s. The quantities g_n are the magnitudes of vectors formed by the addition of two integer multiples of the reciprocal lattice vectors of the surface unit cell, and K_2 and K_5 are modified Bessel functions of the second kind. The potential comprises two distinct parts, a z-dependent summed 10–4 potential (eq 2b), which corresponds physically to smearing the graphite atoms within each basal plane perpendicular to the z axis, and an x-, y-, and z-dependent Fourier series (eq 2c), which accounts explicitly for the local topography of the first graphite layer. The first five terms of this Fourier series are implemented, following the recommendations of Steele.[5] The necessary five g_n coefficients and f_n functions are tabulated in the same reference. In our implementation, the 10–4 sum is performed over the surface and the first 63 underlying layers of graphite atoms only; the remaining potential contribution is then accounted for by smearing the graphite carbons in all three directions, resulting in a 9–3 potential form:[3,4]

$$\mathcal{V}_0(z) = \frac{4\pi\sigma_{ps}^2\epsilon_{ps}}{a_s}\sum_{\alpha=0}^{63}\left[\frac{2}{5}\left(\frac{\sigma_{ps}}{z+\alpha d}\right)^{10} - \left(\frac{\sigma_{ps}}{z+\alpha d}\right)^4\right] + \frac{4\pi\sigma_{ps}^3\epsilon_{ps}}{3a_s d}\left[\frac{2}{15}\left(\frac{\sigma_{ps}}{z+64d}\right)^9 - \left(\frac{\sigma_{ps}}{z+64d}\right)^3\right] \tag{2d}$$

Performing the 10–4 sum for an infinite number of terms

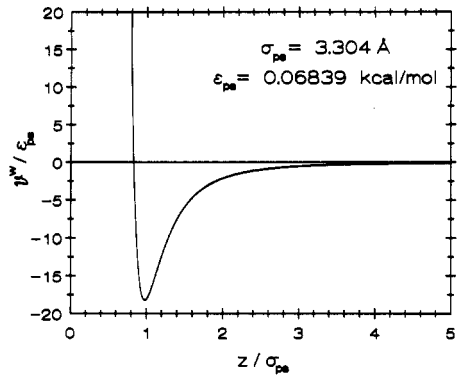

Figure 1. Polymer/graphite potential used during stage IV of the simulation (see text for details). The potential shown here, eq 2, is plotted for a backbone carbon atom that lies directly above the center of a graphite hexagon (i.e., s1 = s2 = 0) as a function of distance z normal to the solid phase.

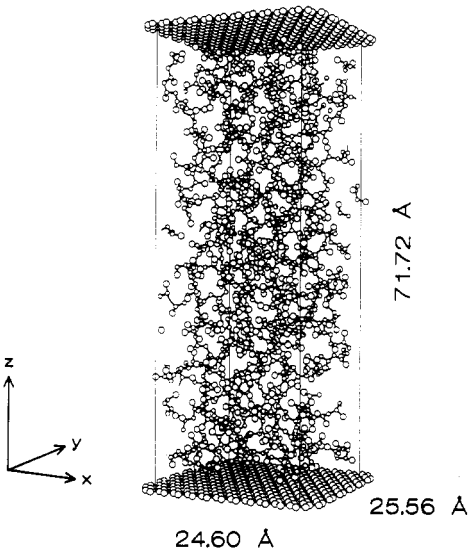

Figure 2. "Relaxed" model structure of a thin film of glassy atactic polypropylene, built from seven $H[CH_2CH(CH_3)]_{76}CH_3$ chains and sandwiched between two basal planes of graphite. Periodic boundary conditions are implemented in the x and y directions. The smaller and larger spheres in the polymer phase correspond to carbons and methyls, respectively. Hydrogens have been omitted, and the displayed atoms have had their van der Waals radii reduced for clarity.

in this manner was found to be more accurate than using the Euler–MacLaurin theorem.[57] K_0 and K_1 are calculated by using polynomial approximations, and from these, the higher order K functions are found by using recursion relationships.[58] Following Steele's recommendations,[5] the graphite potential parameters for the collision diameter and well depth were taken as σ_{ss} = 3.4 Å and ϵ_{ss}/k = 28 K, respectively, where k is the Boltzmann constant. A d = 3.4 Å spacing between the basal planes was also used.[5] All polymer atom/graphite potential parameters (σ_{ps}, ϵ_{ps}) were determined by using the Lorentz–Berthelot combining rules.[59] To give the reader a feeling for the strength of the polymer atom/graphite interaction, we plot in Figure 1 the potential energy felt by a skeletal carbon lying directly above the center of a hexagon in the basal plane of a semiinfinite graphite crystal as a function of its normal distance from the basal plane.

Our computational technique[46,50] calls for the creation of a set of model static graphite/atactic polypropylene/graphite microstates, such as the one shown in Figure 2. A microstate is an orthorhombic cell containing segments from several "parent" chains and characterized by periodic boundary conditions in the x and y directions. It can be viewed as part of a thin film extending to infinity in these directions. The x and y dimensions of the cell must be chosen larger than twice the range of polymer/polymer interatomic interactions and ideally should be considerably larger than the unperturbed root-mean-squared radius of gyration $\langle s^2 \rangle_0^{1/2}$ of constituent chains. The top and bottom faces of the cell are exposed to basal planes of graphite, which extend to infinity on either side of the polymer. We desire that the separation distances of the graphite surfaces be large enough so as to make the middle region of the film behave as a bulk polymer yet small enough to keep computations tractable. Generally,[50] this requires the use of a separation distance (film thickness h) larger than 4 times $\langle s^2 \rangle_0^{1/2}$ in the z direction. We have chosen the x, y, and z dimensions of our model cell as 24.60 Å, 25.56 Å, and h = 71.72 Å, respectively. Note that h is precisely defined in this work as the distance between the top layers of graphite carbon atoms on either side of the polymer film. The above x and y dimensions are commensurate with the graphite lattice; the top and bottom of the model cell are each bounded by 10 × 12 surface unit cells of the basal plane. The semiinfinite graphite phases constraining the polymer film are mirror images of each other with respect to the film midplane. In addition, one must specify the number and molecular weight of the chains. We use seven parent chains of the type $RCHR(CH_2CHR)_{x-1}R$ per cell, where R is a methyl group. Each chain has a degree of polymerization x = 76 and a corresponding molecular weight M = 3214. The chain tacticity is Bernoullian with a fraction of meso dyads w_m = 0.48 as is observed experimentally for equilibrium epimerized atactic polypropylene.[55] The unperturbed root-mean-squared end-to-end distance and radius of gyration of our chains at 233 K are $\langle r^2 \rangle_0^{1/2}$ = 44.4 ± 0.3 Å and $\langle s^2 \rangle_0^{1/2}$ = 18.8 ± 0.1 Å (RIS values), respectively.[46] After relaxation, the above choices of simulation box size, number of chains, and molecular weight result in an average density of 0.892 g/cm^3 in the middle of our microstates; this is the experimental value for the bulk density of atactic polypropylene at 1 atm and 233 K, roughly 20 °C below its glass transition temperature.[55] The bulk density, pressure, temperature, chain tacticity, and molecular weight specifications are the same as in our previous free surface work.[50] Thus, a direct comparison between the model glassy polymer/vacuum and glassy polymer/solid interfaces is possible.

3. Simulation

The underlying assumptions of our simulation, described in section 2 and in our previous work,[50] call for the generation of a set of static microstates, each representative of a local configuration of a thin glassy polymer film adsorbed between two graphite phases. Appropriate functions of configuration of the various microstates are then calculated and arithmetically averaged to obtain estimates of microscopic structural features and thermodynamic properties. Generating a static model microstate entails the very challenging problem of packing chains at a glassy density. As in our previous work,[46,50] we perform this process in two steps. First, an initial guess configuration is generated via a Monte Carlo scheme. Subsequently, the total potential energy of this configuration is minimized with respect to all microscopic degrees of freedom to arrive at a new configuration that satisfies the conditions of detailed mechanical equilibrium. Energy minimization is clearly the most computationally demanding of the two steps, but its CPU (central processing unit) requirements can be significantly reduced by creating initial guess configurations that are close, both structurally and en-

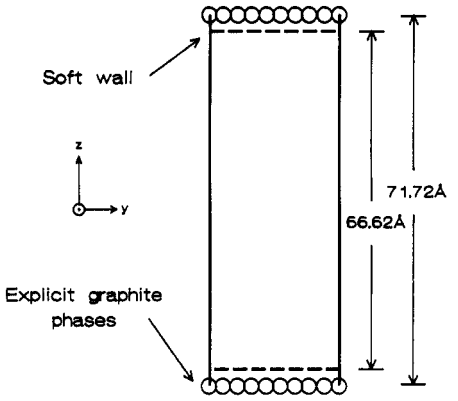

Figure 3. Schematic representation of the location of soft walls relative to the positions of explicit graphite basal planes.

ergetically, to the mimimum energy microstates that will be obtained from them.

The objective of the initial guess generation step is to form a "liquidlike" configuration of realistic density and sufficiently low energy that is situated between two solid phases. Chain configuration must be consistent with short-range intramolecular energetics, excluded volume effects must be accounted for, and chain propagation into the solid phases must be prevented. A Monte Carlo generation approach satisfying these requirements has been developed and described in detail elsewhere;[50] it is briefly reviewed here for convenience.

First, the tacticity of the parent chains is decided upon. Next, the terminal methyl group of each parent chain is randomly placed into the cell. A random orientation is then assigned to the first two skeletal bonds of each chain (i.e., three Eulerian angles are chosen, thus positioning the first five atoms of each parent chain). A strong overlap between any of the initial groups or the placement of a skeletal bond inside a solid phase will cause the initial guess procedure to be discarded at this point and then repeated. Subsequently, the conformations of all parent chains are grown in parallel, bond by bond, by a procedure that resembles polymerization, until their last segments are reached. Two-dimensional periodic boundary conditions are observed during the conformation generation; i.e., whenever a chain exists a face of the box perpendicular to the x or y direction, an identical chain is introduced through the opposite face. The constraining graphite phases prevent chains from exiting through the top and bottom faces of the cell. To simplify the computations in the course of the initial guess generation, we have replaced each explicit graphite phase with the fictitious, steeply repulsive, and smooth "soft-wall" potential used in our previous work.[50] Each soft wall is placed parallel to the top layer of graphite carbon atoms at a distance of 2.55 Å from it toward the film midplane (see Figure 3). The real graphite surfaces are restored later during the potential energy minimization procedure (see below). In the course of the conformation generation, we use a discrete representation of chain conformations, based on Suter and Flory's five-state rotational isomeric state (RIS) model for polypropylene.[55] The conditional probabilities of our Monte Carlo scheme blend the short-range conformational energetics of the RIS model with long-range interactions, so as not to allow chains to cross themselves, each other, or the walls. In the presence of solid walls, we have found it necessary to introduce a new, two-bond scheme for the conformation generation.[50] The rotational state of bond i is decided upon after considering the energetic consequences of placing the bonds i and $i + 1$ in all pairs of states accessible to them. The new scheme allows the chains more freedom to redirect themselves when approaching a steep obstacle.

The initial guess generation is followed by potential energy minimization with respect to all microscopic degrees of freedom. For our system containing $N_c = 7$ parent chains with a degree of polymerization $x = 76$ that are exposed to explicit graphite phases, these are the start coordinates of each chain ($x_{0,i}$, $y_{0,i}$, $z_{0,i}$, where $i = 1, 2, ..., N_c$); three Eulerian angles per chain ($\psi_{1,i}$, $\psi_{2,i}$, $\psi_{3,i}$, where $i = 1, 2, ..., N_c$), specifying the overall orientation with respect to the cell frame of reference; and the sequence of $2x - 2 = 150$ torsion angles for all rotatable bonds of each chain ($\phi_{2,i}$, $\phi_{3,i}$, ..., $\phi_{151,i}$, where $i = 1, 2, ..., N_c$), which define conformation. Each chain has $N_p = 6x - 1 = 455$ atomic groups. Overall, the model system has $N_c(2x + 4) = 1092$ degrees of freedom; this is drastically less than the number that would be required if a fully flexible representation cast in $3N_pN_c = 9555$ Cartesian coordinates were used. We employ a four-stage optimization strategy in this work. We start with a purely repulsive, "soft sphere", polymer/polymer potential and reduced polymer atomic radii (stage I) and proceed by using the same soft sphere potential, but this time using radii of actual size (stage II). Both of these stages are performed in the presence of the soft walls as in ref 50; it does not pay to introduce the actual texture of the substrate surfaces until later stages of the simulation. Minimization in the presence of the soft walls requires 2 fewer degrees of freedom (i.e., $N_c(2x + 4) - 2 = 1090$), since the wall potential is invariant with respect to rigid translation of the polymer film along the x and y axes. During stage III of the minimization, the soft walls are turned off and replaced by xy smeared soft sphere graphite carbon atoms at their actual positions (see Figure 3). This smeared, repulsive solid interacts with a polymer atom through only the z-dependent summed 10–4 potential, eq 2b, up to the point where this potential is zero. The zero point is easily found numerically by the method of bisection; for example, it is $z/\sigma_{ps} = 0.851$ Å for a backbone carbon atom. The attractive part of both the polymer/polymer and the polymer/graphite interatomic interaction potentials is incorporated in the final stage of the minimization, which leads to a fully relaxed model microstate (stage IV). During stage IV, the polymer/graphite potential eq 2a, as developed by Steele,[5] depends on all three polymer atom coordinates. Since interactions of the polymer with the entire semiinfinite graphite phases are included during this stage of the minimization, the "tail" contributions from long-range cohesive interactions over distances larger than the range of interatomic potentials within the polymer[46] must also be incorporated. This is done by modeling the polymer film at large distances from a given atom as a background of uniform density in all three atomic species present (see Appendix A). Neglecting this contribution would bring about an artificial enhancement of polymer density near the solid phases, resulting in incorrect structural features and interfacial thermodynamic properties.

The total potential energy of a static model microstate obtained from the final stage IV of the minimization consists of the sum of the following: all nonbonded van der Waals interactions within the polymer film,[46] including long-range contributions; the intrinsic torsional potentials associated with the skeletal bonds;[46] and the potential interaction of all film atoms with the upper and lower graphite phases (eqs 2a–d). The minimization of the total potential energy function is performed with the quasi-Newton BFGS algorithm,[60] using analytical derivatives.

These derivatives are identical with those derived in previous work,[46,50] except for the fact that the derivatives of the atom/graphite potential expressions, eqs 2a–d, and of the long-range polymer/polymer potential (Appendix A) with respect to all microscopic degrees of freedom are also needed. The minimization algorithm lends itself to extensive vectorization. This feature and other code enhancements, such as the implementation of a Verlet neighbor list[50,59] in the computation of polymer/polymer interactions, make it possible to arrive at a fully relaxed model microstate of atactic polypropylene sandwiched between two basal planes of graphite within 6 CPU h on the 8/864 Cray Y-MP at the San Diego Supercomputer Center. Estimates of the structural features and macroscopic properties of the glassy polymer/graphite interface are obtained by averaging over several static model microstates obtained in this way. In the averaging process, the convergence of structural features at the level of individual segments (e.g., density profile) is much faster than that of thermodynamic estimates. We have found 15 static model microstates to give adequate predictions of the interfacial thermodynamic properties of interest here.

To assess the possibility of model system size effects, we created 35 smaller static model microstates. Each of these microstates contains $N_c = 3$ chains having the same degree of polymerization $x = 76$ and tacticity $w_m = 0.48$ as the chains used in our larger base case simulations. In the smaller microstates, the polymer film lies between two graphite basal planes, which are separated by 66.28 Å, and the simulation box has x and y dimensions of 17.22 and 17.04 Å, respectively. The initial guess generation and potential energy minimization were performed in the same manner as previously described, creating microstates at the same temperature and bulk density as in the larger base case simulations.

4. Results

Thermodynamics. The internal energy contribution to interfacial thermodynamic properties is predicted from our static model microstates based on a statistical mechanical analysis of changes in the interfacial area of contact between polymer and undeformable solid. The fundamental equation of thermodynamics for a macroscopic solid/polymer/solid sandwich, whose middle (bulk) region is isotropic, is derived in Appendix B. The final equation can be written as

$$\mathrm{d}\underline{U} = T\,\mathrm{d}\underline{S} - P\,\mathrm{d}\underline{V} + \mu\,\mathrm{d}n + (\gamma_{sp} - \gamma_s)\,\mathrm{d}\underline{a} \qquad (3)$$

In eq 3, $\underline{U}$ and $\underline{S}$ stand for the internal energy and entropy of the sandwich relative to a pair of graphite phases at the same distance from each other as in our system, with vacuum in between. P is the zz component of the pressure tensor; it coincides with the xx and yy components in the isotropic middle region. $\underline{a}$ is the total interfacial area of contact between polymer and solid (both faces); n is the number of chains in the sandwich, μ is the chemical potential per chain in a bulk glassy polymer phase at temperature T and pressure P. γ_{sp} is the interfacial tension between solid and polymer, and γ_s is the surface tension of a clean graphite surface. The quantity $\gamma_s - \gamma_{sp}$ is sometimes referred to as the "adhesion tension".[61] Through a Maxwell relation on the fundamental equation for the first Legendre transform of $\underline{U}$ with respect to $\underline{S}$, the internal energy part of the adhesion tension can be related to the derivative of the internal energy of the film with respect to surface area at constant T, volume $\underline{V}$, and n:

$$(\gamma_{sp} - \gamma_s)^U \equiv (\gamma_{sp} - \gamma_s) - T\left.\frac{\partial(\gamma_{sp} - \gamma_s)}{\partial T}\right|_{\underline{V},\underline{a},n} = \left.\frac{\partial \underline{U}}{\partial \underline{a}}\right|_{T,\underline{V},n} \approx \left.\frac{\partial \mathcal{V}^0}{\partial \underline{a}}\right|_{\underline{V},n} \qquad (4)$$

The last equality in eq 4 is a direct consequence of eq 1. The quantity $\partial\mathcal{V}^0/\partial\underline{a}|_{\underline{V},n}$ is estimated from our simulations by subjecting each static model microstate to an *infinitesimal affine* deformation, which displaces the graphite phases inwards, while at the same time flattening the film. The components of the strain tensor for this deformation are the same in the x and y directions. The deformation leaves the graphite phases undistorted, increases the area of interfacial contact, but preserves the volume of the film. The associated change in potential energy is calculated from the work done on all polymer atoms (Appendix C). The final expression is

$$(\gamma_{sp} - \gamma_s)^U = -\frac{1}{2\underline{a}}\left\{\sum_i\sum_{j\neq i}\left[\frac{1}{2}(x_i - x_j)_{\min}F^{\min}_{ij,x} + \frac{1}{2}(y_i - y_j)_{\min}F^{\min}_{ij,y} - (z_i - z_j)F^{\min}_{ij,z}\right] + \sum_i\sum_k\left[x_iF_{ik,x} + y_iF_{ik,y} - 2\left(z_i - \frac{h}{2}\right)F_{ik,z}\right] + \sum_i\sum_l\left[x_iF_{il,x} + y_iF_{il,y} - 2\left(z_i + \frac{h}{2}\right)F_{il,z}\right]\right\} \qquad (5)$$

Equation 5 is cast in terms of the interatomic forces and distances within the polymer (indices i and j run over all polymer atoms and min denotes the minimum image convention[59]), as well as all polymer/solid forces (indices k and l run over all atoms in the upper and lower solid phases, respectively). The film thickness h is also involved in eq 5. Given that each microstate is in detailed mechanical equilibrium, one can readily prove that eq 5 is invariant to the coordinate system used.

Experimental data on interfacial thermodynamic properties of the polypropylene/graphite system are not readily available. Fowkes[62] recommends a Girifalco and Good type geometric mean expression for estimating the work of adhesion from the dispersion force contributions to the surface tensions of the two phases involved. Furthermore, he suggests that the work of adhesion is not very sensitive to temperature. Experimental values of the dispersion force contribution to the surface tensions of solid polypropylene and graphite, from equilibrium spreading pressure measurements, are given by Fowkes as $\gamma^d = 28.5$ mN/m and $\gamma_s^d = 123$ mN/m, respectively. Based on these values, the experimental estimate of the work of adhesion[2] is

$$W_{a,exp} = \gamma + \gamma_s - \gamma_{sp} \approx 2(\gamma^d\gamma_s^d)^{1/2} = 118\ \mathrm{mN/m} \qquad (6)$$

By subtracting the surface tension of polypropylene γ, one obtains an experimental estimate of $(\gamma_s - \gamma_{sp})_{exp} = 90$ mN/m for the adhesion tension. No evidence is available on the temperature dependence of either of these quantities. Our model predictions for the internal energy contribution to the adhesion tension (mean value over 15 static model microstates ± 95% confidence limits for the mean value) at 233 K are $(\gamma_s - \gamma_{sp})^U_{theory} = 73 \pm 43$ mN/m. By using our previously reported theoretical prediction for the internal energy contribution to the surface tension of glassy atactic polypropylene,[50] $\gamma^U = 43 \pm 23$ mN/m, the predicted value of the internal energy contribution for

work of adhesion is

$$W^{U}_{a,\text{theory}} = (43 \pm 23) + (73 \pm 43) = 116 \pm 49 \text{ mN/m} \quad (7)$$

which is in very good agreement with the best available experimental value shown in eq 6. Polymer/polymer potential "tail" contributions, due to attractive interactions at long range, have been included in these estimates by direct integration, after "smearing" each atom in each microstate in the x and y directions so that the anisotropic nature of the film is taken into account.[50] One should point out that this comparison between our computed estimates and experimental values is limited by the unavailability of experimental evidence on the temperature dependence of the interfacial thermodynamic quantities.

Methods for calculating the atomic level stress tensors σ_i on an atom i, as well as the local internal stress tensor $\sigma(z)$ over small sections Δz of the films, have been presented.[46,50] The internal energy contribution to the adhesion tension, eq 5, can be expressed as

$$(\gamma_s - \gamma_{sp})^U = -\frac{1}{a}\left\langle \sum_k \left[\frac{\sigma_{xx,k} + \sigma_{yy,k}}{2} - \sigma_{zz,k} \right] \Delta V_k \right\rangle = -\frac{1}{2}\left\langle \sum_k \left[\frac{\sigma_{xx,k} + \sigma_{yy,k}}{2} - \sigma_{zz,k} \right] \Delta z_k \right\rangle \quad (8)$$

where k labels a section of the film with a volume ΔV_k and a thickness Δz_k. The spatial distribution of internal stresses was analyzed by superposing all our model microstates so that the graphite phases coincide. The superposed structures were divided into bins by drawing planes parallel to the solid surfaces. Stresses were assigned to each section of the superposed microstates as follows: The contribution to the stress tensor from forces between a polymer atom and the solid phases was assigned to the bin the polymer atom resided in. The stress contribution from pairwise forces between polymer atoms i,j was treated according to the convention of Harasima.[63,64] If i and j lay in the same bin, their contribution to the internal stress tensor was assigned once to that bin; if i and j lay in two separate bins, half their contribution to the internal stress tensor was assigned to both bins (compare eq 3.11 of ref 63). To improve statistics, we took advantage of the fact that the system is macroscopically symmetric with respect to its midplane. In the following discussion, position z = 0 Å corresponds to the centers of carbon atoms in the top layer of the basal plane of graphite, and position z = 35.86 Å corresponds to the midplane of the polymer film. Plots of σ_{xx}, σ_{yy}, and σ_{zz} across our model graphite/polymer/graphite microstates, including polymer/polymer potential tail contributions,[50] are shown in Figure 4a. All three diagonal components of the internal stress tensor are tensile throughout the film. The xx and yy components are practically coincident with each other, but the zz component is significantly more tensile near the solid phases. Error bars represent 95% confidence limits from averaging over the 15 microstates. The intrinsically anisotropic nature of the interface is clearly seen in the internal stress profiles over a distance larger than an unperturbed root-mean-squared radius of gyration from the graphite. The internal stress tensor in the middle of the static microstates is found to be isotropic within the error of the simulation, confirming that the value of the adhesion tension is dominated by contributions from the anisotropic regions close to the solid phases.

The internal stress tensor of our superposed microstates is composed of polymer/solid and polymer/polymer contributions, which can be easily separated. Their distributions, assigned to bins in the same manner as above, as shown in Figure 4b,c. All diagonal components of the polymer/solid contribution are practically zero in the middle of our microstates; this demonstrates that the presence of the graphite phases is not felt in the middle of the film, which is thus indistinguishable from bulk polymer. However, the polymer/solid stress differs significantly from zero along the zz direction, along which it is strongly tensile, due to the attractive forces between polymer atoms and the graphite. The polymer/polymer contribution to the local internal stress, including long-range tails, is again found to be isotropic in the middle

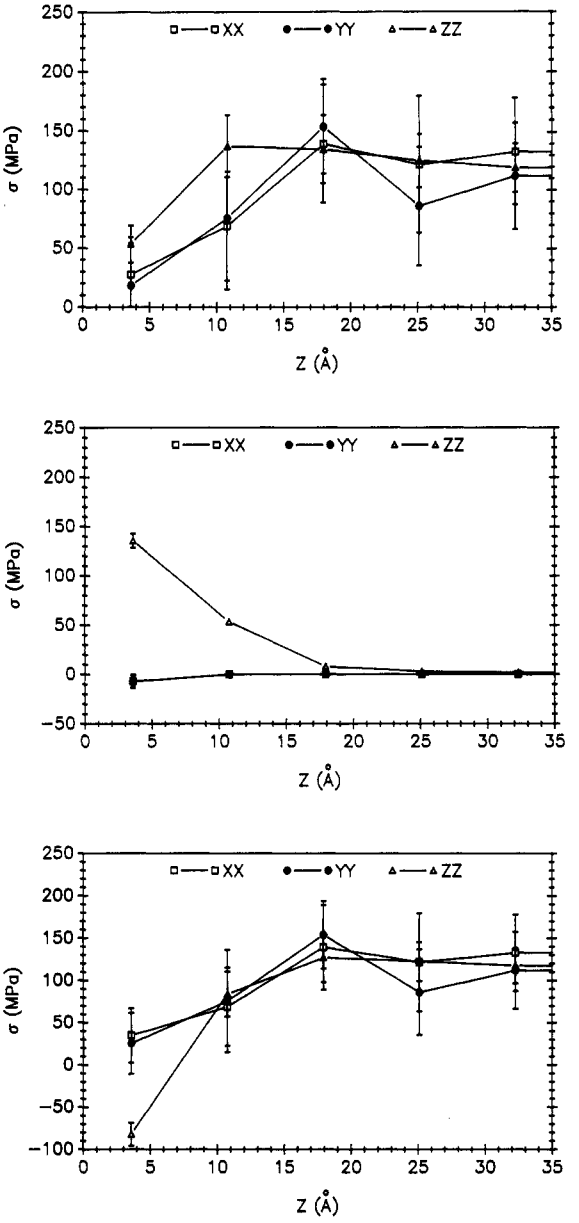

Figure 4. (a, top) Distribution of diagonal components of the local internal stress tensor from a set of 15 model microstates, as defined by eq 7 in the text. The first layer of carbon atoms of the solid is located at z = 0 Å. The anisotropic nature of the local internal stress tensor is clearly seen near the solid phases (extreme left of figure). The middle region of the model polymer film (right-hand side of figure) is mechanically *isotropic*, representative of unperturbed bulk polymer. (b, middle) Polymer/solid contribution to the diagonal components of the local internal stress tensor. The addition of this part and part c results in part a. (c, bottom) Polymer/polymer contribution to the diagonal components of the local internal stress tensor. The plot includes long-range tail contributions.

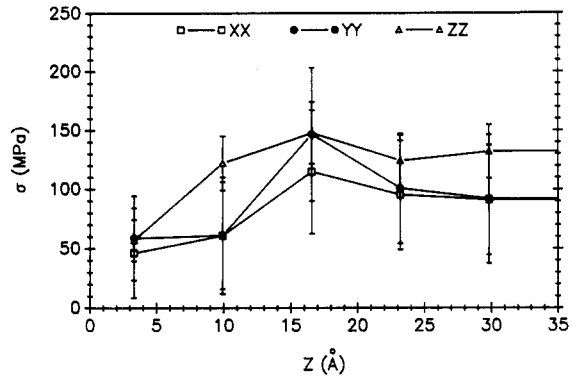

Figure 5. Distribution of diagonal components of the local internal stress tensor obtained from a set of 35 model microstates of small size (see text for details). The stress in the middle of these microstates (extreme right of this figure) is anisotropic, and therefore, the results are subject to system size effects.

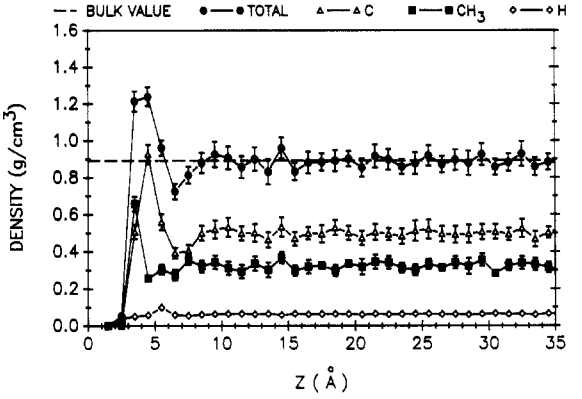

Figure 6. Local mass density distribution at a glassy atactic polypropylene/graphite interface. The solid line indicates the experimentally observed macroscopic density at the simulation temperature. Individual contributions to the mass density profile from skeletal carbon, hydrogen, and methyl groups are also shown.

region. Its zz component is strongly compressive very close to the solid, as polymer segments are pushed together under the influence of the strongly attractive potential field of the solid. The behavior of the internal stress distribution discussed above suggests that the box size used in our base case simulations is sufficiently large for the safe estimation of surface thermodynamic properties.

System size effects have been assessed by comparing the above results for the adhesion tension and for the internal stress distribution to the corresponding results obtained from our set of 35 smaller graphite/polymer/graphite static model microstates. $(\gamma_s - \gamma_{sp})^U_{theory}$ for the smaller microstates is 99 ± 40 mN/m, and the work of adhesion is $W^U_{a,theory}$ = (43 ± 23) + (99 ± 40) = 142 ± 46 mN/m. Although still reasonable, this estimate compares less favorably with experimental evidence, eq 6, than the value predicted from our larger microstates, eq 7. The corresponding internal stress profile across the smaller structures is shown in Figure 5. The middle of the films is clearly mechanically anisotropic, since $\sigma_{xx} \approx \sigma_{yy} \neq \sigma_{zz}$. This means that the middle region contributes substantially to the calculated interfacial properties and indicates that the small microstates are subject to system size effects. The results from these smaller microstates should thus be interpreted with extreme caution. The discussion in the rest of this paper is based on the set of 15 large graphite/polymer/graphite static model microstates (7 chains/simulation box), unless otherwise indicated.

Structure. In addition to thermodynamic properties, how chains organize in the interfacial region is of interest. Structural features were analyzed in the same manner as the internal stress distributions, by superposing all model microstates so that the graphite phases coincide and dividing the resulting structure into bins separated by planes parallel to the solid surfaces. Averages of characteristic structural quantities and associated 95% confidence limits were computed within each bin. Furthermore, the results were averaged over both halves of the superposed structures, taking advantage of symmetry with respect to the film midplane. The structural information to be presented has been analyzed first on the length scale of individual segments and bonds and then on the length scale of entire chains.

Figure 6 displays the mass density distribution across the film, together with its individual components due to skeletal carbon, pendant hydrogen, and methyl groups. The information shown in this figure has been accumulated in 1-Å-thick bins along the z axis. In the middle region of the film, the total density assumes its bulk experimental value. Local density displays a strong maximum next to the highly attractive graphite surfaces. Chains adsorb on the surface through their pendant hydrogen and methyl groups. There is a sharp peak in the methyl density profile at a distance from the basal plane roughly equal to the sum of the van der Waals radii of methyls and graphite carbons. An analogous shoulder peak can be discerned in the hydrogen density profile. Skeletal carbons peak at a somewhat larger distance from the graphite surface, as they are kept away from the graphite by pendant bonds. There is no obvious evidence of oscillatory behavior in the density profile. Oscillatory features have been observed in simulations of simple fluids[25-28] and liquids composed of short freely jointed bead-and-spring chains.[34-37] Apparently, the presence of substituents of different sizes in polypropylene has a structure-breaking effect that causes any oscillations to disappear. On the basis of the perturbations in the total density profile from its bulk value, the thickness of the interface could be estimated as approximately 10 Å. Note that this is significantly less than the interfacial thickness over which the internal stress tensor is anisotropic (Figure 4a).

Local orientational tendencies of bonds are also of interest. We define a bond order parameter S_B = $0.5[3\langle\cos^2\theta\rangle - 1]$ in terms of the angle θ formed between a bond and the direction normal to the surface. S_B would assume a value of −0.5, 0.0, and 1.0 for bonds characterized by perfectly parallel, random, and perpendicular orientation relative to the surface, respectively. Since a chain has fewer bonds than atoms, we accumulated this structural feature in slightly larger 2-Å-thick bins. A given bond is assigned to the bin in which its midpoint resides. The results are plotted in Figure 7. Close to the graphite, one sees a significant tendency for skeletal carbon–carbon bonds to orient parallel to the solid substrate, i.e., S_B = < 0. This tendency is clearly stronger than the corresponding tendency at a free glassy polymer surface.[50] The skeletal bond orientation profile of Figure 7 compares well with the corresponding prediction of a simple, lattice-based, self-consistent-field model of polymer melts near adsorbing solids.[65] Perhaps most interesting is the strongly perpendicular orientation of pendant carbon–hydrogen bonds next to the surface. This suggests some registry between adsorbed hydrogens and the surface.

To explore this idea further, we accumulated two-dimensional surface density maps for adsorbed hydrogens, defined here as hydrogens located less than 3 Å from the graphite phases. The rhombus-shaped surface unit cell of graphite[5] is divided into a 10 × 10 grid by drawing lines

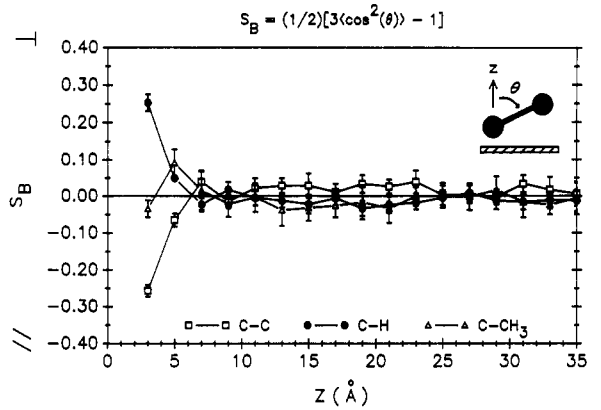

Figure 7. Local order parameter for C–C, C–H, and C–CH_3 bonds as a function of distance from the solid. A positive (negative) order parameter indicates an orientational tendency that is perpendicular (parallel) to the surface planes.

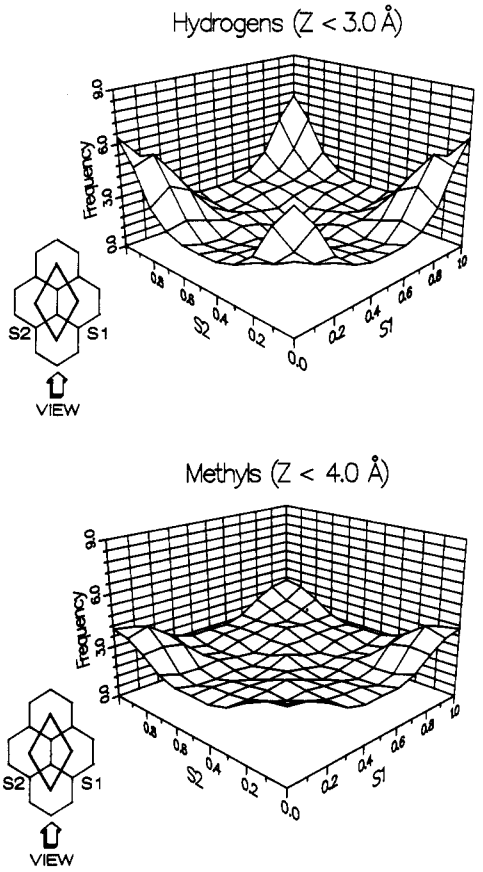

Figure 8. Two-dimensional surface density map for groups adsorbed on the graphite surface. The (s1,s2) domain of the graph constitutes a side view onto the surface unit cell of the graphite basal planes, as indicated in the inset. The plotted function is proportional to the probability that an adsorbed atom will reside above a certain point of the surface unit cell. (a, top) Surface density map for those pendant hydrogens that are within 3 Å of either graphite basal plane. (b, bottom) Surface density map for adsorbed methyls, located within 4 Å of either basal plane.

parallel to its edges. Adsorbed hydrogens are then translated into a reference surface unit cell by addition of appropriate integer multiples of the unit cell's vectors and assigned to one of 100 possible slots. Once all adsorbed hydrogens have been considered, further averaging is performed, taking into account the symmetries of the surface unit cell, as reflected in the polymer/graphite potential (eq 2). We find, as shown in Figure 8a, that hydrogens show a strong tendency to locate themselves above the centers of the graphite hexagons when adsorbed

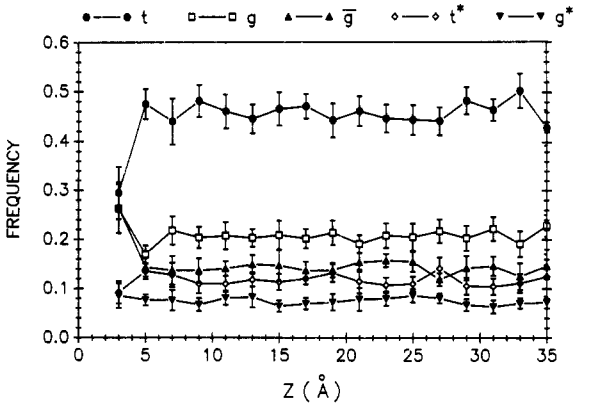

Figure 9. Distribution of torsion angles, assigned to their nearest rotational isomeric state value, as a function of position in the film. The most favored state in the unperturbed bulk, t, is depleted near the graphite phases.

on the surface. A similar plot, shown in Figure 8b, has been prepared for the adsorbed methyl groups. Due to their larger radius, methyls cannot come as close to the graphite phases as the hydrogen atoms. Therefore, the corresponding surface density plot was accomulated within 4 Å of a surface. As shown in Figure 8b, our simulation predicts that adsorbed methyls also display some registry with the graphite surfaces, but to a much lesser extent than the hydrogens. There is no evidence for preferred adsorption of backbone carbon atoms at any distance: This finding is not surprising, since pendant bonds keep the chain backbone atoms farther than 5 Å from each graphite surface, as discussed above (see Figure 6). At this distance, the x and y dependence of the polymer/solid potential[5] has practically subsided.

The anisotropic environment prevailing at an interface has been found to cause the conformational preferences of chains to depart from what they are in the bulk.[50] To assess this effect in the vicinity of our graphite phases, we have calculated the distribution of bond torsion angles, within 2-Å-thick bins, as a function of position of the bond midpoints. Rotation angles were grouped into five rotational states, defined according to the RIS scheme of Suter and Flory.[55] In partitioning bonds among rotational states, we have used the same intervals as in our previous work.[46,50] The probability of each state is presented in Figure 9 as a function of position in the film. Far from the graphite phases, the RIS distribution is consistent with previous bulk work, with the t state being most favored. Near the graphite phases, this state is severely depleted; instead, there is an enhancement of states g and $\bar{g}$, which enable chains approaching the graphite from the bulk region to turn and run parallel to the solid surfaces. This result is in contrast to the molecular dynamics study of monolayer growth of decane on graphite basal planes, performed by Leggetter and Tildesley.[16] These authors observe an increase in trans conformations upon adsorption. A difference between their work and the work reported here is that they deal with monolayers of short chains next to the graphite, while we deal with a bulk phase of long chains, in which the balance between adsorption energy, cohesive energy, and conformational entropy is struck at a much less uniform distribution of conformations. Another difference is that the regular polymethylene nature of their chains, as opposed to the atactic vinyl nature of our chains, would promote the formation of all-trans arrangements on the surface, reminiscent of epitaxially crystallized monolayers. Interestingly, Leggetter and Tildesley do report a decrease in the population of the trans state with increasing surface coverage. According to our simulations,

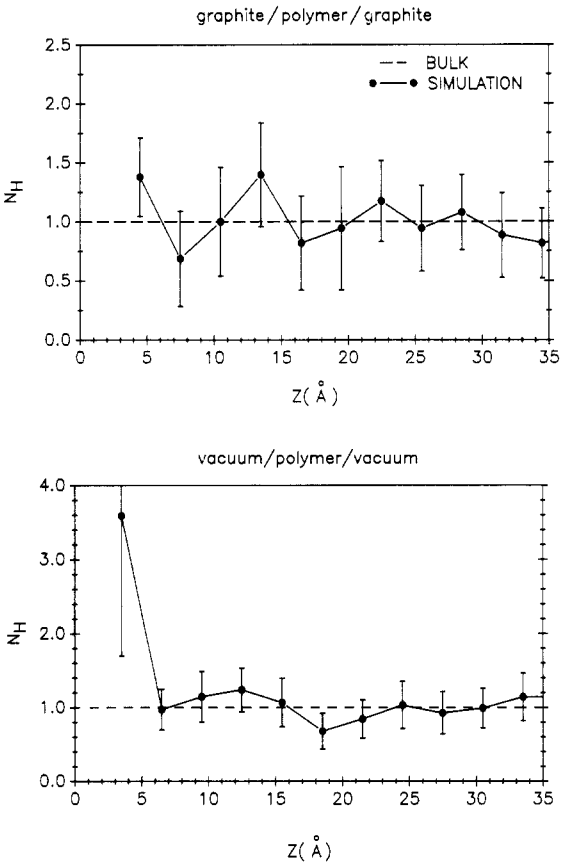

Figure 10. (a, top) Normalized chain head density profile for glassy atactic polypropylene adsorbed on basal planes of graphite. (b, bottom) Normalized head density profile at the free surface of glassy atactic polypropylene, from calculations reported in ref 50.

perturbations in the torsion angle distribution relative to its bulk characteristics again appear to be confined to the immediate vicinity of the graphite walls (less than 10 Å from each graphite surface).

The presence of a phase boundary gives rise to entropic constraints on chain conformation. Exposing the heads, or ends, of the chains to the surface represents a smaller entropic cost than exposing middle segments.[65] Based on this argument, the ends might be expected to concentrate preferentially near the solid surface. We define the normalized polymer head distribution N_H as

$$N_H(z) = \frac{N^c \rho_H(z)}{2\rho(z)} \tag{9}$$

where $\rho_H(z)$ and $\rho(z)$ correspond to the number densities of chain ends and of polymer segments in the bin centered at z, respectively. N^c is the total number of polymer segments per chain. This result, shown in Figure 10a, suffers from poor statistics as our system has only $2N_c$ = 14 chain ends per cell. The error bars barely allow one to state that there is a mild enhancement in the concentration of chain ends next to the graphite (not exceeding 35%). This finding is in qualitative agreement with the more conclusive molecular dynamics results of Bitsanis and Hadziioannou[37] and the Monte Carlo work of Yethiraj and Hall.[36] It is interesting to compare this normalized head distribution against the corresponding distribution at the free surface of a glassy polymer. The latter, accumulated from 70 static model microstates of a free glassy film of atactic polypropylene,[50] is shown in Figure 10b. Clearly, there is a much stronger tendency for chain ends to segregate to the surface in the case of a polymer/vacuum interface than in the case of a polymer/adsorbing solid interface. This observation is consistent with the predictions of a simple self-consistent-field approach to polymer melts at interfaces and can be explained in terms of a balance between enthalpic and entropic factors.[65]

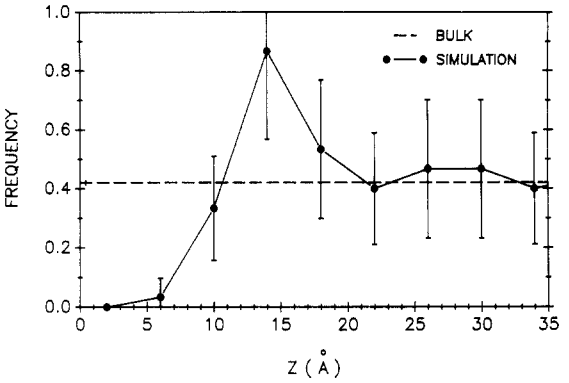

Figure 11. Chain center of mass distribution, accumulated in 3-Å-thick bins. The maximum occurs at somewhat less than 1 unperturbed radius of gyration from the graphite phases.

In addition to local structure at the level of segments and bonds, longer range structural features at the level of entire chains are also of interest. An important length scale for chains at this level of description is their unperturbed root-mean-squared radius of gyration $\langle s^2 \rangle_0^{1/2}$. Our microstates each contain seven parent chains; the results at the level of the entire chains are therefore subject to more statistical uncertainty than segment and bond-level results. An example of a structural feature at this level of description is how the chains as entire objects distribute themselves between the graphite phases. One way of tagging an entire chain is by its center of mass. The spatial distribution of chain centers of mass, calculated in 4-Å-thick bins, is shown in Figure 11. There is a depletion of chain centers of mass near the solid: since chains are finite objects, their centers of mass cannot come arbitrarily close to the surface. Associated with this exclusion effect, there is a peak in the distribution, observed at a distance somewhat less than $\langle s^2 \rangle_0^{1/2}$ from the graphite phases. The center of mass distribution of chains at a free surface[50] also displays a primary peak at the interface. A comparison of the two distributions reveals that the peak position lies slightly closer to the extreme edge of the polymer in the case of a solid/polymer interface than in the case of a vacuum/polymer interface.

The average number N_s of segments per chain participating in a certain region of the microstates is indicative of the "width" of the chains in that region:[50]

$$N_s(z) = \rho(z)/\rho_c(z) \tag{10}$$

In eq 10, ρ_c is the number density of chains passing through the bin. As one moves from the graphite surfaces toward the bulk, the width of chains first rises sharply, reaching a maximum near z = 6 Å, and then decays to an asymptotic bulk value (Figure 12). The chains are seen to be flattened in the presence of the solid phases, over a distance of approximately $1.5\langle s^2 \rangle_0^{1/2}$. This finding is in quantitative agreement with the prediction of a simple self-consistent-field model of polymer melt/solid interface.[65] This behavior could be accounted for in two ways: either the intrinsic shape of chain segment clouds is distorted (i.e., chains near the solid, when looked at in their principal axis system, are more disklike or even rodlike than chains in the bulk), or chains simply reorient themselves as entire objects with respect to the surfaces.

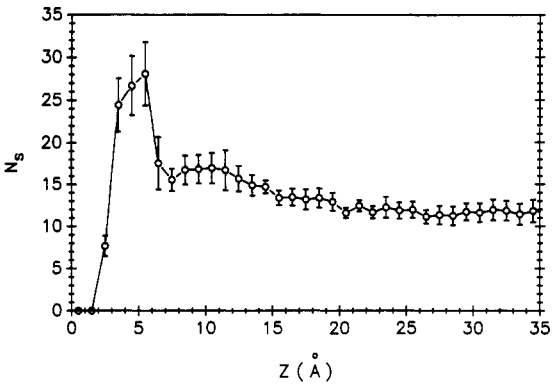

Figure 12. Average width of chains plotted as a function of position. The distribution, accumulated in 1-Å-thick bins, shows an increase in the average width of chains parallel to the film plane near the graphite surfaces.

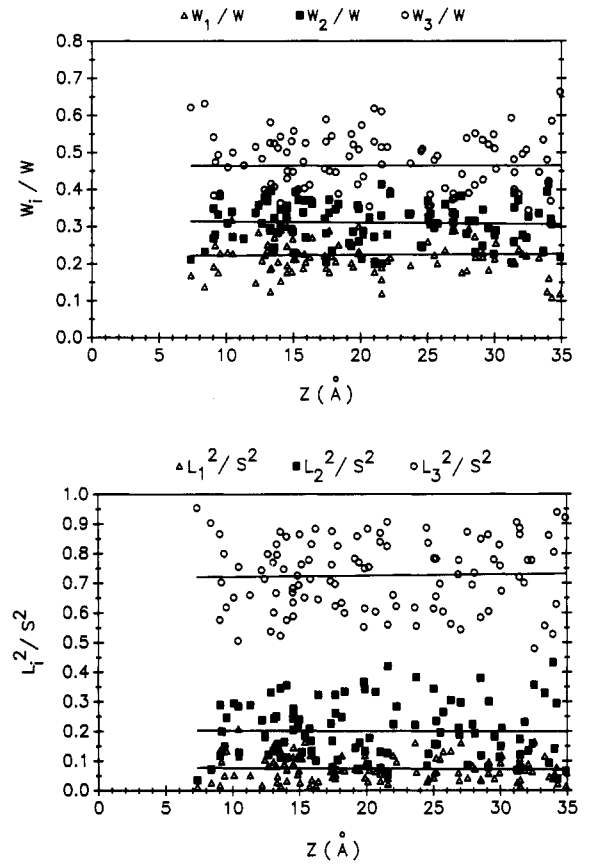

Figure 13. Overall shape of chains as a function of center of mass position. (a, top) Spans of chains, normalized by their sum $W = W_1 + W_2 + W_3$. (b, bottom) Eigenvalues of the chain radius of gyration tensor, normalized by their sum $s^2 = L_1^2 + L_2^2 + L_3^2$. Straight lines have been drawn by least-squares regression of the data in both figures. These plots reveal that the overall shape of chain segment clouds is practically independent of position.

We explored the overall shape of chains by determining their spans and the eigenvalues of their radius of gyration tensors. Spans are defined following Rubin and Mazur[50,66] as the dimensions of the smallest orthorhombic box that can completely enclose the chain segment cloud. Our analysis, presented for both spans and eigenvalues in Figure 13, leads to the conclusion that the overall shape of the segment cloud, when looked at in the reference frame of the principal axes, remains virtually unaffected by the presence of an adsorbing solid surface. How chain segment clouds tend to *orient* in the interfacial region is a different question, which we explored by computing order parameters for chain spans as in our previous free surface work.[50]

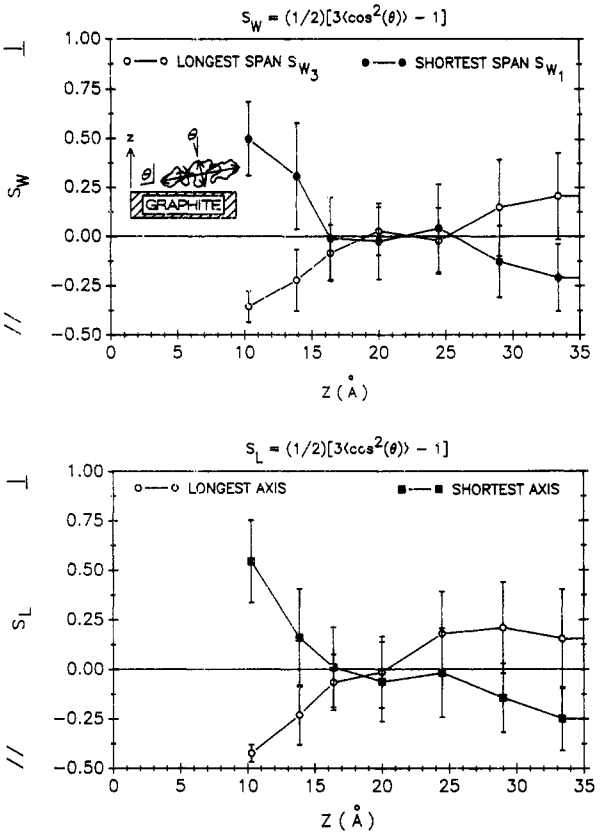

Figure 14. (a, top) Order parameters for the longest and shortest spans of chains as functions of center of mass position. Each point represents an average over 15 model chains. (b, bottom) Order parameters for the eigenvectors corresponding to the largest and smallest eigenvalues of the chain radius of gyration tensor as functions of the center of mass position for all chains encountered in our static model microstates. Each point represents an average over 15 model chains.

The definition of the order parameter for spans is analogous to that used here for the bonds. Plotted in Figure 14a are the order parameters for the shortest and longest span as functions of chain center of mass position. In the interfacial region, we see a strongly tendency for the longest span to orient parallel to the surface and for the shortest span to orient perpendicular to the surface. This tendency remains unchanged if, instead of spans, one uses the principal axes of inertia (i.e., the eigenvectors of the radius of gyration tensor) as measures of shape (Figure 14b). The reorientation of chains is confined to a region whose width is commensurate with $\langle s^2\rangle_0^{1/2}$.

The microscopic structure of the 35 smaller microstates was probed in exactly the same manner as the aforementioned larger base case simulations. Structural features at the level of segments and bonds, such as density, bond orientation, and torsion angle profiles, are virtually identical between the two cases. This is not surprising, since these features vary over a length scale of approximately 10 Å, which is smaller than all three dimensions of the model box in both cases. However, structural features that reflect the location, shape, and size of the chains, such as center of mass, span, and span orientation distributions, differ significantly between the two system sizes studied. As shown above, these features are governed by a length scale commensurate with overall chain dimensions, i.e., the radius of gyration. The x and y dimensions of the model box in the small system case are roughly equal to $\langle s^2\rangle_0^{1/2}$. This introduces an artificial registry of the chains with their periodic images, which affects chain shape.[50]

5. Conclusions

We have used a detailed atomistic molecular mechanics approach to simulate a glassy polymer/solid interface. Although our implementation of this approach focused on interfaces between glassy atactic polypropylene and graphite, the method is quite general and can be applied to more complex systems. Our predictions for interfacial thermodynamic properties, namely the internal energy contribution to the adhesion tension, and to the work of adhesion are within 20% of the best available experimental values. The polymer density is strongly enhanced near the graphite surface. Perturbations in local segment density, bond orientation, and torsion angle distribution from isotropy are confined to a narrow region at the interface that is approximately 10 Å thick. The crystal structure of the graphite surface induces some organization among adsorbed pendant groups. The chain center of mass distribution exhibits a well-defined peak at a distance somewhat less than 1 unperturbed root-mean-squared radius of gyration from the solid surface. In addition, chains close to the solid phases tend to lie flat, with their longest dimension parallel to the interface. Finally, all structural features and thermodynamic predictions have been investigated for possible model system size effects. Interfacial thermodynamic properties, such as the distribution of internal stresses and the work of adhesion, and structural features at the level of entire chains, such as chain orientation, can be estimated safely only when the model system dimensions are significantly larger than $\langle s^2 \rangle_0^{1/2}$, while the local density, bond orientation, and conformation angle distributions are rather insensitive to the model system size.

The local microscopic structure of a glassy polymer/solid interface, as revealed by the simulation reported herein, has been compared to the corresponding structure of a free glassy polymer surface studied in our previous work.[50] This comparison provides quantitative information on the similarities and differences between these two types of interfaces. The polymer density profile next to a vacuum phase is sigmoidal, as opposed to exhibiting a maximum near an adsorbing solid surface. The tendency of backbone bonds to orient parallel to the surface is stronger in the solid/polymer case than in the free surface case. Backbone bonds of chains at the edge of a free polymer film have a random orientation, while backbone bonds situated very close to a solid prefer to align parallel to the surface. The distribution of bond torsion angles in both systems shows a depletion of the usually dominating t state in the interfacial region. The interfacial thickness, based on the anisotropy of structure at the level of segments and bonds, is approximately 10 Å in both cases. The chain center of mass distributions both display a primary peak located at a distance of approximately $\langle s^2 \rangle_0^{1/2}$ from the corresponding solid or vacuum phase; this peak is located slightly closer to the phase boundary in the polymer/solid case. Overall chain shape and size, as characterized by spans and eigenvalues of the radius of gyration tensor, are not significantly affected by the presence of an interface. Chains near a solid or vacuum phase tend to reorient themselves so that their longest dimension aligns parallel to the surface plane. The organization of chains is perturbed relative to the bulk over a region whose thickness is commensurate with approximately $1.5\langle s^2 \rangle_0^{1/2}$ in both interfacial systems studied.

Acknowledgment. This work was supported by the Director, Office of Energy Research, Office of Basic Energy Sciences, Materials Science Division of the U.S. Department of Energy under Contract No. DE-AC03-76SF00098. We also thank E. I. du Pont de Nemours & Co., the Union Carbide Corporation, and BP America for generous gifts. We are grateful to Cray Research, Inc., for making our computations possible through University Research and Development Grants between 1987 and 1990. We thank the San Diego Supercomputer Center, where all computations were performed, for excellent technical support. D.N.T. expresses gratitude to the National Science Foundation for a 1988 P.Y.I. Award, No. DMR-8857659.

Appendix A. Derivation of Long-Range Polymer/Polymer Interatomic Interaction Potential Contribution

The polymer/graphite interatomic interaction potential used in this work, developed by Steele,[5] expresses the potential felt by a polymer atom due to all layers of carbon centers in a semi-infinite graphite phase. This potential exerts a strong attractive force on all polymer atoms except those located at distances extremely close to the solid, which feel repulsion. This adhesive force competes, in a sense, against the cohesive interactions within the polymer. Here and in our previous work,[46,50] polymer/polymer interatomic interactions are represented as pairwise additive; the dominant short-range contribution to those interactions is calculated explicitly from a 6–12 Lennard-Jones potential that has been truncated and smoothed to zero by using a quintic spline. Since Steele's method[5] incorporates the full, infinite-range interaction between polymer and solid, the long-range tail contribution to polymer/polymer cohesive forces must also be included during the creation of static model microstates. Otherwise, an artificial imbalance would arise between adhesive and cohesive interactions, which would make the former appear too strong. In our earlier free surface work,[50] we described how to calculate the tail correction to the thermodynamic properties of a polymer film (e.g., surface tension), in a manner that takes into account the actual density profile in the film. This technique, which could be used directly in this work, takes an image of a specific polymer atom and smears it in the x and y directions parallel to the surface. It is employed in postprocessing our simulation results for the adhesion tension calculations. Use of this procedure to deal with the potential tail corrections during the course of our minimization calculations would be very demanding in computer time, as it necessitates consideration of all polymer atom pairs (and not only minimum image pairs). Thus, we chose to simplify this potential evaluation by assuming a uniform density distribution throughout the film for the purpose of evaluating the tail contributions.

Consider a system, with periodic boundary conditions imposed in the x and y directions, that contains an atom i located somewhere between two solid phases separated by a distance h (in the following, the index i will be used to signify both the considered atom and its type). Next, consider all the atoms of type j that lie closer to the first atom than the atom/atom interatomic potential range R_{ij}.[46,50] Further, let $R_{1,ij}$ be the distance from a given atom i where the full 6–12 Lennard-Jones potential $\mathcal{V}_{ij}^{LJ}$ is replaced with a quintic spline potential.[46] We now wish to calculate the contribution to the potential energy of the system due to interactions between atom i and all the j atoms that lie outside the sphere of radius R_{ij}, as well as a correction to the potential energy due to interactions between i and all j atoms lying at a distance $R_{1,ij}$ to R_{ij} from i. For a bulk system, the long-range potential energy felt by atom i from all atoms of type j would be expressed

as the following integral:[46,59]

$$\mathcal{V}_{ij}^{\text{tails}} = 4\pi\rho_j \int_{R_{1,ij}}^{\infty} r^2\, dr\, g_{ij}(r)\, \Delta\mathcal{V}_{ij}(r) \qquad (A.1)$$

g_{ij} is the ij pair distribution function, which is often assumed to be unity for distances larger than $R_{1,ij}$, and ρ_j is the number density of atoms of type j. $\Delta\mathcal{V}_{ij}(r)$ is defined as the difference $\mathcal{V}_{ij}^{LJ}(r) - \mathcal{V}_{ij}^{NB}(r)$ at a separation distance r. $\mathcal{V}_{ij}^{NB}$ is the finite-range interatomic interaction potential employed in our explicit summation of pairwise interactions (including the spline contribution), and $\mathcal{V}_{ij}^{LJ}$ is the full Lennard-Jones interatomic potential function. Obviously, $\mathcal{V}_{ij}^{NB} = 0$ at r values greater than R_{ij}. Applying eq A.1 to an interfacial system, such as that of a polymer exposed to two solid surfaces, would clearly be incorrect since, as a result of the finite width of the film, the polymer atom i does not see a spherically symmetric density distribution of j atoms around it. The integration over all j atoms between the solid phases[67] can be accomplished easily if the domain of integration is broken up into two regions, one where the j atoms lie outside of our finite ranged potential, i.e., $\mathcal{V}_{ij}^{NB} = 0$, and one where the j atoms interact explicitly with atom i. The contribution to atom i from the first region can be calculated from

$$\mathcal{V}_{ij}^{I} = 2\pi\rho_j \int_0^h dz \int_{\max(R_{ij},|z-z_i|)}^{\infty} r\, dr\, \mathcal{V}_{ij}^{LJ}(r) \qquad (A.2)$$

The contribution from the second region, which corrects for atoms j that have been included in the short-range potential energy summation with atom i by using a spline function instead of the full Lennard-Jones potential, can be calculated from

$$\mathcal{V}_{ij}^{II} = 2\pi\rho_j \int_{\max(0,z_i-R_{ij})}^{\min(h,z_i+R_{ij})} dz \int_{\max(R_{1,ij},|z-z_i|)}^{R_{ij}} r\, dr\, \Delta\mathcal{V}_{ij}(r) \qquad (A.3)$$

The long-range potential energy experienced by atom i from all atoms of type j is formed from the sum of eqs A.2 and A.3. The total tail contribution to the polymer/polymer cohesive energy is calculated by summing over all atoms i and all atom types j and dividing by 2 to correct for double counting of the interactions:

$$\mathcal{V}^{\text{tails}} = \frac{1}{2} \sum_{\substack{\text{all} \\ \text{atoms } i}} \sum_{\substack{\text{all} \\ \text{types } j}} (\mathcal{V}_{ij}^{I} + \mathcal{V}_{ij}^{II}) \qquad (A.4)$$

The derivatives of eq A.4 with respect to all microscopic degrees of freedom are needed for our total potential energy minimization technique. These are found by first calculating the derivative of eq A.4 with respect to z_i and then using a simple chain rule as described previously.[46,50]

Appendix B. Thermodynamic Analysis of Solid/Polymer/Solid System

We derive here the fundamental equation, eq 3, for our polymer film sandwiched between two solid surfaces. Our thermodynamic formulation follows the work of Magda et al.[25] on a simple liquid-filled slit. As shown in Figure 15, we consider a polymer film p between two completely involatile, incompressible, and undeformable solid phases s, separated by a distance h. The total solid-film contact area is $\underline{a}$, or $\underline{a}/2$ per solid phase. This solid-film combination is in equilibrium with a surrounding bath of bulk polymer b at a pressure, temperature, and chemical potential of P_b, T, and μ_b, respectively. The solids can be considered as attached to the upper and lower walls of this bath by springs. Let $\underline{V}_{p+b}$ be the total volume of polymer in the film and bulk regions and P_b the pressure in the (isotropic) bulk region. The internal energy change

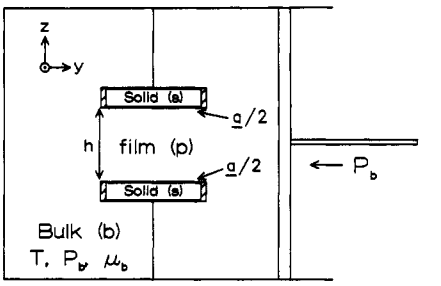

Figure 15. Phases considered in the thermodynamic analysis of a polymer film between two undeformable solids.

of the entire system (encompassing solid, film, and bulk polymer) associated with a infinitesimal change in state can be written[25] as

$$d\underline{U}_{s+p+b} = T\, d\underline{S}_{s+p+b} - P_b\, d\underline{V}_{p+b} + \mu_b\, dn_{p+b} + (P_b - P_N)\underline{a}\, dh/2 + \gamma_{sp}\, d\underline{a} \qquad (B.1)$$

In eq B.1, $\underline{S}_{s+p+b}$ is the entropy of the entire system, n_{p+b} is the number of moles of polymer in the film and bulk regions, γ_{sp} is the interfacial tension, and P_N is the normal component of the pressure tensor in the film between the two solids. For large enough h, the middle region of the film is indistinguishable from the bulk; $P_b - P_N$ is zero, and the term containing it can be dropped. Consider now the same system at the same temperature T but with the polymer everywhere replaced by vacuum. Given our assumption of incompressibility and undeformability of the solid phases, the internal energy change associated with an infinitesimal change of state of this new solid/vacuum system can be expressed as

$$d\underline{U}_s = T\, d\underline{S}_s + \gamma_s\, d\underline{a} \qquad (B.2)$$

In eq B.2, $\underline{U}_s$ and $\underline{S}_s$ symbolize the internal energy and entropy of the solid phases, and γ_s is the surface tension of the solid exposed to vacuum. Furthermore, under our assumptions regarding the solid phase, the contribution from the solid to the quantities $d\underline{U}_{s+p+b}$ and $d\underline{S}_{s+p+b}$ during the change considered in eq B.1 will be identical with the quantities $d\underline{U}_s$ and $d\underline{S}_s$ of eq B.2, provided the relative position and spatial extent of the solid phases is the same at the beginning and end of both thermodynamic changes. By subtracting eq B.2 from eq B.1, after setting $P_b - P_N$ to zero, we obtain

$$(d\underline{U}_{s+p+b} - d\underline{U}_s) = T(d\underline{S}_{s+p+b} - d\underline{S}_s) - P_b\, d\underline{V}_{p+b} + \mu_b\, dn_{p+b} + (\gamma_{sp} - \gamma_s)\, d\underline{a} \qquad (B.3)$$

or

$$d\underline{U}_{p+b} = T\, d\underline{S}_{p+b} - P_b\, d\underline{V}_{p+b} + \mu_b\, dn_{p+b} + (\gamma_{sp} - \gamma_s)\, d\underline{a} \qquad (B.4)$$

Equation B.4 involves the thermodynamic properties of the polymer and the adhesion tension of the polymer/solid system. Note that $d\underline{U}_{p+b}$ contains the potential energies associated with cohesive polymer/polymer and adhesive polymer/solid forces, but has no contribution at all from cohesive solid/solid forces or forces between the two solid phases across the gap. Dropping the subscript p + b for simplicity we obtain eq 3 in the main text.

Appendix C. Derivation of the Internal Energy Contribution to the Adhesion Tension for a Bonded System (Equation 5)

The formulation follows our previous modeling work on the free surface of bonded systems.[50] Consider a film of polymer p placed between two solid surfaces s_1 and s_2,

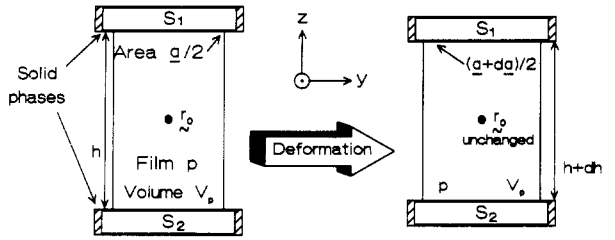

Figure 16. Affine deformation considered in the energy analysis of Appendix C. The two graphite surfaces are brought closer together, while the polymer film is flattened so as to preserve its total volume. Although an infinitesimally small deformation is used in the actual calculation, a much larger deformation is shown here for clarity. A calculation of the reversible work associated with this process serves as the basis for estimating the adhesion tension.

which interact with one another and with the polymer through pairwise additive nonbonded (central) forces. In addition, some of the film atoms are connected by infinitely stiff bonds and experience bonded (not necessarily central) forces and torques.[46] Imagine subjecting this system to a reversible infinitesimal deformation that (a) moves the solids closer together, (b) leaves the solid phases undistorted, and (c) preserves the volume of the film by increasing the solid/film contact area, as demonstrated in Figure 16. The mechanical work done by all polymer/polymer forces and torques and all polymer/solid forces (compare eq B.4 and subsequent discussion in Appendix B) can be written[46] as

$$\bar{d}W = \sum_{i\in p}\left(\sum_{\substack{j\in p\\ j\neq i}}\mathbf{F}_{ij} + \sum_{k\in s_1}\mathbf{F}_{ik} + \sum_{l\in s_2}F_{il}\right)\cdot d\mathbf{r}_i + \sum_{i\in p}\left(\sum_{\substack{j\in p\\ j\neq i}}\mathbf{T}_{ij}^{B}\right)\cdot\left[\frac{1}{2}(\nabla\times d\mathbf{r})\right]_i + \sum_{k\in s_1}\left(\sum_{i\in p}\mathbf{F}_{ki}\right)\cdot d\mathbf{r}_k + \sum_{l\in s_2}\left(\sum_{i\in p}\mathbf{F}_{li}\right)\cdot d\mathbf{r}_l \quad (C.1)$$

$\mathbf{F}_{ij}$ is the total force on atom i due to j, including both bonded and nonbonded contributions, and $\mathbf{T}_{ij}^{B}$ represents the bonded torque on atom i due to j. For the purpose of estimating the rate of change of $\bar{d}W$ with deformation, it is a satisfactory approximation[46,50] to assume that the coordinates of all atoms in the system undergo *an infinitesimal affine deformation*:

$$\mathbf{r}_i^{affine} = \mathbf{A}\mathbf{r}_i + \mathbf{b} \quad (C.2)$$

The strain tensor ϵ is related to the transformation matrix $\mathbf{A}$ by

$$\epsilon = \frac{1}{2}(\mathbf{A}^T\mathbf{A} - \mathbf{I}) \approx \frac{1}{2}(\mathbf{A}^T + \mathbf{A}) - \mathbf{I} \quad (C.3)$$

For the polymer film atoms, whose deformation leaves the directions of the film axes unchanged and preserves the volume of the p phase, the strain tensor has the following diagonal form:

$$\epsilon = \begin{bmatrix}\epsilon_{xx} & 0 & 0\\ 0 & \epsilon_{yy} & 0\\ 0 & 0 & \epsilon_{zz}\end{bmatrix} \qquad \epsilon_{xx} + \epsilon_{yy} + \epsilon_{zz} = 0 \quad (C.4)$$

Equation C.2 for the atoms of the polymer film can be written in terms of ϵ as

$$d\mathbf{r}_i^{affine} = \epsilon\cdot(\mathbf{r}_i^{undeformed} - \mathbf{r}_0) \quad (C.5)$$

where $\mathbf{r}_0$ is the position of the centerpoint of the film, which is a fixed point of the transformation. The solid atoms undergo rigid displacement along the z axis. Their new positions for the upper and lower solids can be expressed as

$$\mathbf{r}_k^{affine} = \mathbf{r}_k^{undeformed} + \frac{h}{2}\epsilon_{zz}z\hat{z} = \mathbf{r}_k^{undeformed} - \frac{h}{2}(\epsilon_{xx} + \epsilon_{yy})z\hat{z} \quad (C.6)$$

$$\mathbf{r}_l^{affine} = \mathbf{r}_l^{undeformed} + \frac{h}{2}(\epsilon_{xx} + \epsilon_{yy})z\hat{z} \quad (C.7)$$

where $\hat{z}$ the unit vector along the z axis. The change in contact area between the film and both solid phases can be expressed in terms of ϵ as

$$d\underline{a} = \underline{a}(\epsilon_{xx} + \epsilon_{yy}) \quad (C.8)$$

Substituting eqs C.5–C.8 in eq C.1, taking advantage of the reciprocity of pairwise interatomic interactions, setting the work equal to the negative change of the potential energy of the film, and employing the result of our thermodynamic-statistical mechanical analysis (eq 4), one readily derives the equation

$$(\gamma_{sp} - \gamma_s)^U = \frac{-1}{2\underline{a}}\sum_{i\in p}\sum_{\substack{j\in p\\ j\neq i}}\left[\frac{\epsilon_{xx}}{\epsilon_{xx}+\epsilon_{yy}}(x_i - x_j)F_{ij,x} + \frac{\epsilon_{yy}}{\epsilon_{xx}+\epsilon_{yy}}(y_i - y_j)F_{ij,y} - (z_i - z_j)F_{ij,z}\right] - \frac{1}{\underline{a}}\sum_{i\in p}\sum_{k\in s_1}\left[\frac{\epsilon_{xx}}{\epsilon_{xx}+\epsilon_{yy}}x_iF_{ik,x} + \frac{\epsilon_{yy}}{\epsilon_{xx}+\epsilon_{yy}}y_iF_{ik,y} - \left(z_i - \frac{h}{2}\right)F_{ik,z}\right] - \frac{1}{\underline{a}}\sum_{i\in p}\sum_{l\in s_2}\left[\frac{\epsilon_{xx}}{\epsilon_{xx}+\epsilon_{yy}}x_iF_{il,x} + \frac{\epsilon_{yy}}{\epsilon_{xx}+\epsilon_{yy}}y_iF_{il,y} - \left(z_i + \frac{h}{2}\right)F_{il,z}\right] \quad (C.9)$$

This result is independent of the center of the deformation, because of the fact that the film is in detailed mechanical equilibrium in the undeformed state. For $\epsilon_{xx} = \epsilon_{yy}$, one gets a simpler expression:

$$(\gamma_{sp} - \gamma_s)^U = \frac{-1}{2\underline{a}}\sum_{i\in p}\sum_{\substack{j\in p\\ j\neq i}}\left[\frac{1}{2}(x_i - x_j)F_{ij,x} + \frac{1}{2}(y_i - y_j)F_{ij,y} - (z_i - z_j)F_{ij,z}\right] - \frac{1}{\underline{a}}\sum_{i\in p}\sum_{k\in s_1}\left[\frac{1}{2}x_iF_{ik,x} + \frac{1}{2}y_iF_{ik,y} - \left(z_i - \frac{h}{2}\right)F_{ik,z}\right] - \frac{1}{\underline{a}}\sum_{i\in p}\sum_{l\in s_2}\left[\frac{1}{2}x_iF_{il,x} + \frac{1}{2}x_iF_{il,y} - \left(z_i + \frac{h}{2}\right)F_{il,z}\right] \quad (C.10)$$

Equation C.10 holds for a macroscopic (nonperiodic) system only. When incorporating periodic boundary conditions in the x and y directions, one has a great number N_f of replicas of the central box in place of a macroscopic film. The atom–atom interactions in the periodic film are active between nearest-neighbors only, resulting in the following simplification:

$$\sum_{i\in p}\sum_{\substack{j\in p\\ j\neq i}}(x_i - x_j)F_{ij,x} = \sum_{i\in p}\sum_{\substack{j\in p\\ j\neq i}}(x_i - x_j)_{min}F_{ij,x}^{min} = N_f\sum_{i\in box}\sum_{\substack{j\in box\\ j\neq i}}(x_i - x_j)_{min}F_{ij,x}^{min} \quad (C.11)$$

and similarly for the y and z direction: along the latter, $(z_i - z_j)_{min} \equiv z_i - z_j$. All images of the film atoms lie over

crystallographically equivalent positions of the solid surfaces, so that

$$\sum_{i\in p} x_i F_{ik,x} = \sum_{i\in \text{box}} \sum_{\substack{i',\text{all} \\ \text{images of i}}} x_{i'} F_{i'k,x} = \sum_{i\in \text{box}} F_{ik,x}\Big(\sum_{\substack{i',\text{all} \\ \text{images of i}}} x_{i'}\Big) = N_f \sum_{i\in \text{box}} x_i F_{ik,x} \quad \text{(C.12)}$$

and similarly for the y and z direction and for the lower solid. In these summations, the translation vectors along x and y used for forming the images i' from the position i in the box cancel for symmetric pairs of images. In addition, the interfacial area of the film is a multiple of the interfacial area of the box:

$$\underline{a} = N_f \underline{a}_{\text{box}} \quad \text{(C.13)}$$

Using eqs C.10–C.13, one can confine the sums over the film atoms to the primary box only, arriving at the equation

$$(\gamma_{sp} - \gamma_s)^U = \frac{-1}{2\underline{a}_{\text{box}}} \sum_{i\in p} \sum_{\substack{j\in p \\ j\neq i}} \Big[\frac{1}{2}(x_i - x_j)_{\min} F^{\min}_{ij,x} + \frac{1}{2}(y_i - y_j)_{\min} F^{\min}_{ij,y} - (z_i - z_j) F^{\min}_{ij,z} \Big] - \frac{1}{\underline{a}_{\text{box}}} \sum_{i\in p} \sum_{k\in s_1} \Big[\frac{1}{2} x_i F_{ik,x} + \frac{1}{2} y_i F_{ik,y} - \Big(z_i - \frac{h}{2}\Big) F_{ik,z} \Big] - \frac{1}{\underline{a}_{\text{box}}} \sum_{i\in p} \sum_{l\in s_2} \Big[\frac{1}{2} x_i F_{il,x} + \frac{1}{2} y_i F_{il,y} - \Big(z_i + \frac{h}{2}\Big) F_{il,z} \Big] \quad \text{(C.14)}$$

which is eq 5 in the main text. The fact that images farther and farther from the center of the deformation would slide more and more with respect to the graphite surface lattice does not give rise to any complications in this result. This stems from the fact that the polymer film is initially in detailed mechanical equilibrium in a configuration commensurate with the graphite surface lattice and also from the infinitesimal nature of the considered deformation.

References and Notes

(1) Kinloch, A. J. *Adhesion and Adhesives: Science and Technology*; Chapman and Hall: New York, 1987.
(2) Wu, S. *Polymer Interface and Adhesion*; M. Dekker: New York, 1982.
(3) Steele, W. A. *The Interaction of Gases with Solid Surfaces*; Pergamon Press: Oxford, 1974.
(4) Nicholson, D.; Parsonage, N. G. *Computer Simulation and the Statistical Mechanics of Adsorption*; Academic Press: London, 1982.
(5) Steele, W. A. *Surface Sci.* **1973**, *36*, 317.
(6) Pisani, C.; Ricca, F.; Roetti, C. *J. Phys. Chem.* **1973**, *77*, 657.
(7) Rybolt, T. R.; Pierotti, R. A. *J. Chem. Phys.* **1979**, *70*, 4413.
(8) Kim, H. Y.; Cole, M. W. *Phys. Rev. B* **1987**, *35*, 3990.
(9) Cheng, A. L.; Steele, W. A. *Langmuir* **1989**, *5*, 600.
(10) Gooding, R. J.; Joos, B.; Bergersen, B. *Phys. Rev. B* **1983**, *27*, 7669.
(11) Koch, S. W.; Abraham, F. F. *Phys. Rev. B* **1986**, *33*, 5884.
(12) Severin, E. S.; Tildesley, D. J. *Mol. Phys.* **1980**, *41*, 1401.
(13) Phillips, J. M.; Hruska, C. D. *Phys. Rev. B* **1989**, *39*, 5425.
(14) Moller, M. A.; Klein, M. L. *J. Chem. Phys.* **1989**, *90*, 1960.
(15) Nosé, S.; Klein, M. L. *Phys. Rev. Lett.* **1984**, *53*, 818.
(16) Leggetter, S.; Tildesley, D. J. *Mol. Phys.* **1989**, *68*, 519; *Ber. Bunsen-Ges. Phys. Chem.* **1990**, *94*, 285.
(17) Joshi, Y. P.; Tildesley, D. J. *Mol. Phys.* **1985**, *55*, 999.
(18) Vernov, A. V.; Steele, W. A. *Langmuir* **1986**, *2*, 219.
(19) Steele, W. A.; Vernov, A. V.; Tildesley, D. J. *Carbon* **1987**, *1*, 7.
(20) Suh, S. H.; O'Shea, S. F. *Can. J. Chem.* **1988**, *66*, 955.
(21) Cheng, A.; Steele, W. A. *J. Chem. Phys.* **1990**, *93*, 3858, 3867.
(22) Bondi, C.; Baglioni, P.; Taddei, G. *Chem. Phys.* **1985**, *96*, 277.
(23) Bondi, C.; Taddei, G. *Surf. Sci.* **1988**, *203*, 587.
(24) Baukema, P. R.; Hopfinger, A. J. *J. Polym. Sci.* **1982**, *20*, 399.
(25) Magda, J. J.; Tirrell, M.; Davis, H. T. *J. Phys. Chem.* **1985**, *83*, 1888.
(26) Snook, I. K.; van Megen, W. *J. Chem. Phys.* **1980**, *72*, 2907.
(27) Abraham, F. F. *J. Chem. Phys.* **1978**, *68*, 3713. Abraham, F. F. *Rep. Prog. Phys.* **1982**, *45*, 1113 and references therein.
(28) Schoen, M.; Diestler, D. J.; Cushman, J. H. *J. Chem. Phys.* **1987**, *87*, 5464. MacElroy, J. M. D.; Suh, S. H. *Mol. Phys.* **1987**, *60*, 475.
(29) Buch, D. H.; Kabadi, V. N. Presented at the 1988 Annual Meeting of the American Institute of Chemical Engineers, Washington, DC, Nov 1988; paper 101G.
(30) Madden, W. G. *J. Chem. Phys.* **1987**, *87*, 1405; **1988**, *88*, 3934.
(31) ten Brinke, G.; Ausserré, D.; Hadziioannou, G. *J. Chem. Phys.* **1988**, *89*, 4374. van Vliet, J. H.; ten Brinke, G. *J. Chem. Phys.* **1990**, *93*, 1436.
(32) Mansfield, K. F.; Theodorou, D. N. *Macromolecules* **1989**, *22*, 3143.
(33) Fitzgibbon, D. R.; McCullough, R. L. *J. Polym. Sci.* **1989**, *27*, 655.
(34) Kumar, S. K.; Vacatello, M.; Yoon, D. Y. *J. Chem. Phys.* **1988**, *89*, 5206; *Macromolecules* **1990**, *23*, 2189; Vacatello, M.; Yoon, D. Y. *J. Chem. Phys.* **1990**, *93*, 779.
(35) Lastoskie, C.; Madden, W. G. *Polym. Prep., Am. Chem. Soc., Div. Polym. Chem.* **1989**, *30* (2), 39.
(36) Yethiraj, A.; Hall, C. K. *J. Chem. Phys.* **1989**, *91*, 4827; *Macromolecules* **1990**, *23*, 1865.
(37) Bitsanis, I.; Hadziioannou, G. *J. Chem. Phys.* **1990**, *92*, 3827.
(38) Cosgrove, T.; Heath, T.; van Lent, B.; Leermakers, F.; Scheutjens, J. *Macromolecules* **1987**, *20*, 1692. Cosgrove, T.; Finch, N. A.; Webster, J. R. P. *Macromolecules* **1990**, *23*, 3353.
(39) Chakrabarti, A.; Toral, R. *Macromolecules* **1990**, *23*, 2016.
(40) Murat, M.; Grest, G. S. *Macromolecules* **1989**, *22*, 4054.
(41) Reiter, J.; Zifferer, G.; Olaj, O. F. *Macromolecules* **1990**, *23*, 224.
(42) Vacatello, M.; Yoon, D. Y. *Polym. Prep., Am. Chem. Soc., Div. Polym. Chem.* **1989**, *30* (2), 74.
(43) Balazs, A. C.; Huang, K.; Lantman, C. W. Presented at the 33rd IUPAC Symposium on Macromolecules, Montreal, Canada, 1990; session 2.9.5.
(44) Fox, J. R.; Andersen, H. C. *J. Chem. Phys.* **1984**, *88*, 4019.
(45) Rigby, D.; Roe, R. J. *J. Chem. Phys.* **1987**, *87*, 7285; **1988**, *89*, 5280.
(46) Theodorou, D. N.; Suter, U. W. *Macromolecules* **1985**, *18*, 1467; **1986**, *19*, 139; **1986**, *19*, 379.
(47) Ludovice, P. J.; Suter, U. W. *Polym. Prep., Am. Chem. Soc., Div. Polym. Chem.* **1987**, *28* (2), 295.
(48) Hutnik, M.; Argon, A. S.; Suter, U. W. *Polym. Prep., Am. Chem. Soc., Div. Polym. Chem.* **1989**, *30* (2), 36.
(49) Sylvester, M. F.; Yip, S.; Argon, A. S. *Polym. Prep., Am. Chem. Soc., Div. Polym. Chem.* **1989**, *30* (2), 32.
(50) Mansfield, K. F.; Theodorou, D. N. *Macromolecules* **1990**, *23*, 4430.
(51) Mansfield, K. F.; Theodorou, D. N. In *Computer Simulation of Polymers*; Roe, R. J., Ed.; Prentice-Hall: Englewood Cliffs, NJ, 1991.
(52) Stillinger, F. H.; Weber, T. A. *Science* **1984**, *225*, 983. Weber, T. A.; Stillinger, F. H. *Phys. Rev. B* **1985**, *31*, 1954.
(53) Gō, N.; Scheraga, H. *Macromolecules* **1976**, *9*, 535.
(54) Bondi, A. *Physical Properties of Molecular Crystals, Liquids and Glasses*; Wiley: New York, 1968.
(55) Suter, U. W.; Flory, P. J. *Macromolecules* **1975**, *8*, 765.
(56) Flory, P. J. *Statistical Mechanics of Chain Molecules*; Interscience Publishers: New York, 1969.
(57) Steele, W. A. *J. Phys. Chem.* **1978**, *82*, 817.
(58) Abramowitz, M.; Stegun, I. A. *Handbook of Mathematical Functions*; Dover Publications, Inc.: New York, 1972; pp 376, 379.
(59) Allen, M. P.; Tildesley, D. J. *Computer Simulation of Liquids*; Clarendon Press: Oxford, 1987.
(60) Hillstrom, K. Nonlinear Optimization Routines in AMDLIB. Technical Memorandum No. 297, 1976; Argonne National Laboratory, Applied Mathematics Division, Argonne, IL; Subroutine GQBFGS in AMDLIB 1976.
(61) Voorhis, J. J.; Craig, R. G.; Bartell, F. E. *J. Phys. Chem.* **1957**, *61*, 1513.
(62) Fowkes, F. M. *Ind. Eng. Chem.* **1964**, *56* (12), 40.
(63) Walton, J. P. R. B.; Tildesley, D. J.; Rowlinson, J. S.; Henderson, J. R. *Mol. Phys.* **1983**, *48*, 1357.
(64) Nijmeijer, M. J. P.; Bakker, A. F.; Bruin, C. *J. Chem. Phys.* **1988**, *89*, 3789.
(65) Theodorou, D. N. *Macromolecules* **1989**, *22*, 4578, 4589.
(66) Rubin, J. R.; Mazur, J. *Macromolecules* **1977**, *10*, 139.
(67) Rowlinson, J. S.; Widom, B. *Molecular Theory of Capillarity*; Oxford University Press: Oxford, 1989.